

Long-range Order in a Short-range Quasi-2D XY Model

Minghui Hu,^{1,2,*} Chao Zhang,^{1,2,*} Dajun Zhang,^{1,2} Yanan Sun,^{1,2} Youjin Deng,^{3,4,†} and Jian-Ping Lv^{1,2,5,‡}

¹Department of Physics, Anhui Normal University, Wuhu, Anhui 241000, China

²Anhui Province Key Laboratory for Control and Applications of Optoelectronic Information Materials, Anhui Normal University, Wuhu, Anhui 241000, China

³Department of Modern Physics, University of Science and Technology of China, Hefei, Anhui 230026, China

⁴Hefei National Laboratory, University of Science and Technology of China, Hefei 230088, China

⁵Key Laboratory of Functional Molecular Solids, Ministry of Education, Wuhu, Anhui 241000, China

The phase of spins in the quasi-two-dimensional (Q2D) XY model has emerged as a topic of significant interest across multiple physics subfields. Here, we propose a short-range (SR) Q2D XY model defined on a plane perpendicularly intersected by a group of parallel planes, with each plane consisting of nearest-neighbor-coupled XY spins. We perform large-scale Monte Carlo simulations to establish the full phase diagram of the Q2D XY model, aided by finite-size scaling. A long-range (LR) ordered phase emerges in the Q2D model when the spins on the parallel planes develop a Berezinskii-Kosterlitz-Thouless critical phase. In the LR ordered phase, ordering is anisotropic: LR correlations develop along the direction of the intersection lines, while critical correlations emerge perpendicular to them. Furthermore, the LR ordered phase exhibits Goldstone-mode physics. Our study hence reveals the existence of LR order in a Q2D XY model with finite SR couplings and opens up a new avenue to explore superfluid orders in low dimensions.

Introduction. The two-dimensional (2D) XY model—a prototype model of superfluidity—plays a vital role in the study of critical phenomena. While the nearest-neighbor spin-spin coupling J of the 2D XY model varies continuously, the Berezinskii-Kosterlitz-Thouless (BKT) transition occurs at $J = J_{\text{BKT}}$ [1]. Albeit the Mermin-Wagner theory forbids long-range (LR) order at any finite J , a quasi-long-range (QLR) order emerges at $J > J_{\text{BKT}}$. When LR couplings are turned on, LR order survives at finite couplings [2], though debates persist regarding phase diagrams [3–6].

Recently, the surface and interface critical phenomena of the 3D XY model have attracted considerable attention [7–12]. The systems of interest can be viewed as quasi-two-dimensional (Q2D) XY models coupled to a critical bulk. LR order is forbidden by a recently proposed no-go theorem in the context of boundary conformal theory for continuous symmetry breaking [12]. Indeed, the extraordinary-log (E-Log) critical phase—characterized by the non-trivial power-law decay with the logarithm of distance for the two-point correlation function—has been found in the surfaces and interfaces of XY models [13–17] and other $O(n)$ systems [18–23]. The E-Log critical phase was also theoretically realized with quantum measurements [24, 25] and quantum hall bilayers [26]. Contrasting to the no-go theorem, for the 3D $O(n)$ model with $n \geq 2$, it was predicted [27] that the surface of tricritical bulk can host LR order. This result was considered the first example of continuous symmetry breaking in two dimensions [27]. However, an updated abstract, from the same authors, presents a different result: the E-Log critical phase exists [28].

Transverse quantum fluid (TQF) is a quantum phase of matter that was originally related to the edge dislocations of superfluid ^4He [29–32]. TQF differs from traditional superfluid by exhibiting infinite compressibility, quadratic normal mode

spectra as well as off-diagonal LR order and demonstrating the irrelevance of Landau criterion [33]. TQF has been realized in 1D quantum lattice models of interacting bosons coupled to a bath [30–32, 34, 35]. The advances in TQF further motivate the search for LR order in a classical superfluid system like the Q2D XY model.

Main Results. The construction of our setup is illustrated by Fig. 1(a), where a square-lattice Q2D XY model (V plane) is perpendicularly intersected by a group of square-lattice XY models (P planes). The XY spins in the setup are interacted via ferromagnetic nearest-neighbor couplings. The Hamiltonian of the setup reads

$$\mathcal{H}/(k_{\text{B}}T) = - \sum_{\langle \mathbf{r}\mathbf{r}' \rangle} J_{\mathbf{r}\mathbf{r}'} \vec{S}_{\mathbf{r}} \cdot \vec{S}_{\mathbf{r}'}, \quad (1)$$

where $\vec{S}_{\mathbf{r}}$ represents an XY spin at lattice site \mathbf{r} , $J_{\mathbf{r}\mathbf{r}'}$ denotes coupling strength, and the summation runs over pairs of nearest-neighbor sites. For the nearest-neighbor sites \mathbf{r} and \mathbf{r}' , $J_{\mathbf{r}\mathbf{r}'}$ obeys

$$J_{\mathbf{r}\mathbf{r}'} = \begin{cases} W, & \mathbf{r} \in V \text{ and } \mathbf{r}' \in V, \\ K, & \mathbf{r} \notin V \text{ or } \mathbf{r}' \notin V. \end{cases} \quad (2)$$

For each of the $(L + 1)$ square lattices, a V plane and L P planes, periodic boundary conditions are imposed along (x, y) or (y, z) directions. For $K = 0$, the V plane reduces to a standard square-lattice XY model, which features a BKT transition at $W = J_{\text{BKT}}$ ($J_{\text{BKT}} \approx 1.11996$ [36]).

Using extensive Monte Carlo simulations, we map out the full phase diagram of the setup, which is shown in Fig. 1(b). For $0 < W < J_{\text{BKT}}$, the Q2D XY model—V plane—experiences iterative transitions as K varies continuously, whereas for $W > J_{\text{BKT}}$, it exhibits a single transition. For $K > J_{\text{BKT}}$ —the P planes are critical—the Q2D XY model enters a LR ordered phase, where y lines are LR ordered but x lines remain critical. The LR order of y lines further exhibits Goldstone-mode physics. These observations provide

* M.H. and C.Z. contributed equally to this work.

† yjdeng@ustc.edu.cn

‡ jplv2014@ahnu.edu.cn

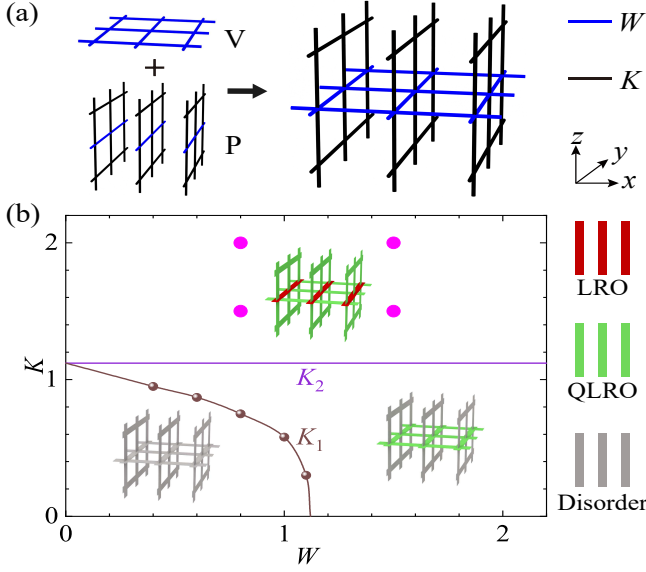


Figure 1. Setup and phase diagram. (a) Construction of the setup, which consists of a vertical (V) plane and L parallel (P) planes, with each plane containing L^2 sites. The V plane is now a $L = 3$ Q2D XY model. The blue and black edges represent the couplings in and out of V plane, with the coupling strengths W and K , respectively. (b) Phase diagram of the setup. For $0 < W < J_{\text{BKT}}$, the V plane experiences a transition at K_1 ($K_1 < J_{\text{BKT}}$) and enters a LR ordered phase at K_2 ($K_2 = J_{\text{BKT}}$), with $J_{\text{BKT}} \approx 1.11996$ the critical coupling of standard square-lattice XY model. The brown spheres represent the transitions at K_1 , which are located at $(W, K) \approx (0.4, 0.95)$, $(0.6, 0.87)$, $(0.8, 0.75)$, $(1, 0.58)$ and $(1.10, 0.3)$. For $W > J_{\text{BKT}}$, the V plane experiences a transition from the QLR to LR ordered phase at K_2 . Each P plane experiences a BKT transition at K_2 from the disordered to QLR ordered phase. The columnar patterns mark the phases of V and P planes, which can be the LR and QLR ordered phases as well as the disordered phase. The phases of V plane at the magenta solid dots are analyzed with Figs. 4 and 5.

the first piece of conclusive evidence that LR order exists in a short-range (SR) Q2D XY model. Remarkably, the present scenario is drastically different from TQF. Here, the “transverse” superfluid (flowing along x direction) is critical rather than has a LR order, whereas LR ordering emerges along y direction.

Method. We perform equilibrium Monte Carlo simulations of model (1) using Wolff’s single-cluster algorithm [37], with linear lattice sizes up to $L = 256$ (maximum number of spins: $L^3 = 16777216$). In the process of cluster growth, for the edge between a pair of nearest-neighbor sites (say \mathbf{r} and \mathbf{r}'), a bond is randomly placed on with the probability $p = \max[0, 1 - e^{-2J_{\mathbf{r}\mathbf{r}'} S_{\mathbf{r}}^{(\alpha)} S_{\mathbf{r}'}^{(\alpha)}}]$, where α is a randomly chosen direction. When the cluster growth is finished, the spins in the cluster are flipped along α direction. For $L = 256$, the maximum number of created clusters reaches 3.1×10^8 ; details are given in Supplemental Material (SM).

Iterative Phase Transitions. We start with analyzing y lines. In the case $W = 0.8$ and $K = 0$, the V plane is in a disordered

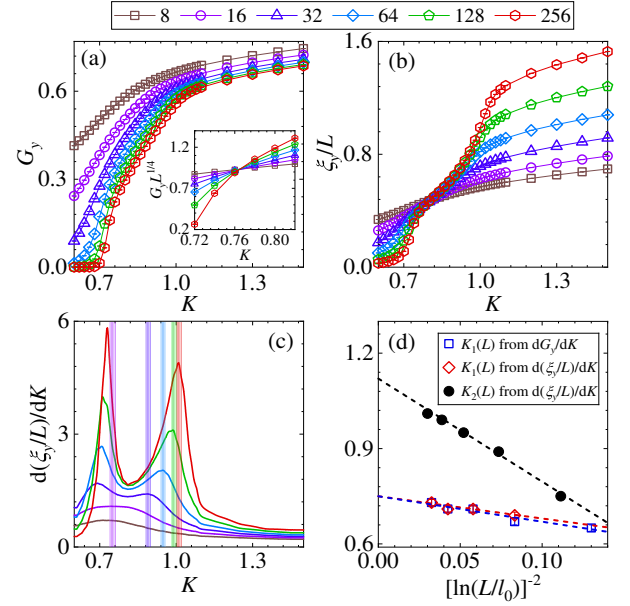


Figure 2. Phase transitions of a y line in the V plane with $W = 0.8$. (a) The large-distance spin-spin correlation G_y versus K . Inset: $G_y L^{1/4}$ versus K . (b) The reduced correlation length ξ_y/L versus K . (c) The derivative $d(\xi_y/L)/dK$ versus K . The shadowed areas, whose widths represent two error bars, denote $K_2(L)$ (the coordinate of the peak at larger K) and $d(\xi_y/L)/dK$ as well as $K_2(L)$ from $d(\xi_y/L)/dK$ versus $[\ln(L/l_0)]^{-2}$. Conforming to fits, $l_0 = 1$ and 0.8 are set for $K_1(L)$ and $K_2(L)$, respectively. The intercepts $K_1 = 0.75$ and $K_2 = 1.11996$ represent the thermodynamic limits of $K_1(L)$ and $K_2(L)$, respectively.

phase. We turn on the coupling $K > 0$ within the P planes. For a line along y direction of the V plane, we sample the large-distance spin-spin correlation $G_y = \langle \vec{S}_{\mathbf{r}} \cdot \vec{S}_{\mathbf{r}+(0,L/2)} \rangle$. Figure 2(a) shows that G_y increases with K . Using the finite-size scaling (FSS) form $G_y \sim L^{-1/4}$ [38] of a BKT transition, we infer a transition point at $K_1 \approx 0.76$ [inset of Fig. 2(a)]. We then compute the second-moment correlation length $\xi_y = (2 \sin \frac{\pi}{L})^{-1} \sqrt{\frac{\langle M_y^2 \rangle}{\langle M_{yk}^2 \rangle}} - 1$ with $M_y = L^{-1} |\sum_{\mathbf{r} \in a y \text{ line}} \vec{S}_{\mathbf{r}}|$ and $M_{yk} = L^{-1} |\sum_{\mathbf{r} \in a y \text{ line}} \vec{S}_{\mathbf{r}} e^{i \frac{2\pi}{L} y}|$, where the summation runs over sites in a y line. Figure 2(b) implies that, as L increases, the reduced correlation length ξ_y/L changes drastically at K_1 and $K_2 \approx 1.1$. In the intermediate regime $K_1 < K < K_2$, ξ_y/L tends to be scale-invariant, indicating the existence of QLR order.

Figure 2(c) demonstrates that the derivative $d(\xi_y/L)/dK$ has a double-peaked structure. For each L , we define a pair of pseudo-critical points $K_1(L)$ and $K_2(L)$ with $K_1(L) < K_2(L)$, which are the K coordinates of the two peaks. Considering the slow convergence of $K_1(L)$ and $K_2(L)$ in the $L \rightarrow \infty$ limit, we perform least-squares fits according to the scaling formula [39]

$$K_n(L) = K_n + a[\ln(L/l_0)]^{-2} \quad (3)$$

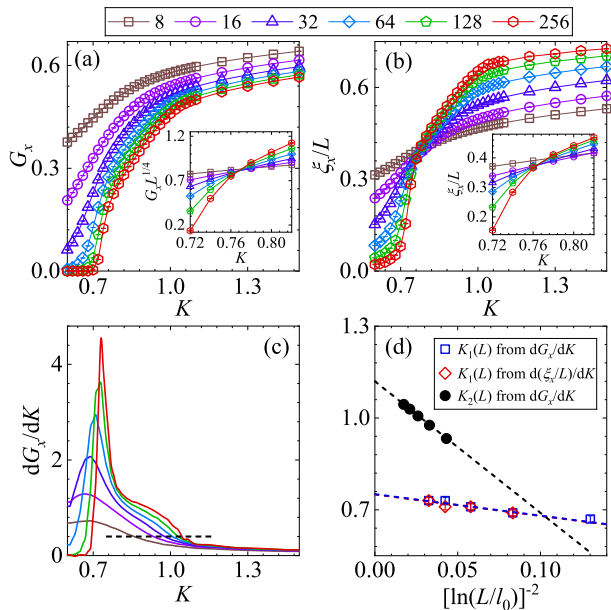


Figure 3. Phase transitions of an x line in the V plane with $W = 0.8$. (a) The large-distance spin-spin correlation G_x versus K . Inset: $G_x L^{1/4}$ versus K . (b) The reduced correlation length ξ_x/L versus K . Inset: a zoom-in plot. (c) The derivative dG_x/dK versus K . The dashed line represents $dG_x/dK = 0.4$. (d) $K_1(L)$ from dG_x/dK and $d(\xi_x/L)/dK$ as well as $K_2(L)$ from dG_x/dK versus $[\ln(L/l_0)]^{-2}$. Conforming to fits, $l_0 = 1$ and 0.13 are set for $K_1(L)$ and $K_2(L)$, respectively. The intercepts $K_1 \approx 0.750$ and $K_2 = 1.11996$ represent the thermodynamic limits of $K_1(L)$ and $K_2(L)$, respectively.

with $n = 1$ and 2 respectively, where a denotes a non-universal constant and l_0 represents a reference length. Throughout this Letter, we examine the quality and stability of fits by monitoring χ^2/DOF upon gradually increasing L_{\min} , with χ^2 standard chi-squared, DOF the degree of freedom, and L_{\min} the lower bound of L . We prefer the fits with $\chi^2/\text{DOF} = O(1)$. Assuming the transition at K_1 is of the BKT type, by fixing $l_0 = 1$ —neglecting effective finite-size corrections and reducing uncertainties—we obtain $K_1 = 0.75(1)$ and $\chi^2/\text{DOF} \approx 0.5$ with $L_{\min} = 32$. For $K_2(L)$, the fit with free l_0 yields $K_2 = 1.07(2)$ and $\chi^2/\text{DOF} \approx 0.1$ with $L_{\min} = 16$. The estimated K_2 is close to $J_{\text{KBT}} \approx 1.11996$ [36]. If $K_2 = 1.11996$ is fixed, a preferred fit is obtained, producing $l_0 = 0.8(2)$ and $\chi^2/\text{DOF} \approx 0.9$ with $L_{\min} = 16$. Additionally, Fig. 2(a) indicates that dG_y/dK is peaked at $K_1(L)$, for which a preferred fit produces $K_1 = 0.750(10)$ and $\chi^2/\text{DOF} \approx 1.0$ with $L_{\min} = 16$. Hence, the methodology is verified via the consistency of estimated K_1 from G_y , $d(\xi_y/L)/dK$ and dG_y/dK . For $n = 1$ and 2 , Fig. 2(d) illustrates the linear dependence of $K_n(L)$ on $[\ln(L/l_0)]^{-2}$ as well as the $L \rightarrow \infty$ limit of $K_n(L)$.

We proceed to consider an x line with $W = 0.8$. Figure 3(a) shows that the large-distance correlation $G_x = \langle \vec{S}_r \cdot \vec{S}_{r+(L/2,0)} \rangle$ varies drastically at K_1 . For $K < K_1$, G_x decays fast to zero in the $L \rightarrow \infty$ limit, indicat-

Table I. The power-law exponent q of Goldstone mode for the 1D LR order in the V plane. The estimates are extracted from preferred least-squares fits of G_y , $\langle M_y^2 \rangle$, $\langle M_{yk}^2 \rangle$ and ξ_y according to Eqs. (5), (6) and (7).

Parameters	q from G_y	q from $\langle M_y^2 \rangle$	q from $\langle M_{yk}^2 \rangle$	q from ξ_y
P ₁	0.523(1)	0.521(4)	0.5321(10)	0.533(2)
P ₂	0.5204(8)	0.508(4)	0.537(7)	0.52(1)
P ₃	0.528(2)	0.5074(8)	0.516(2)	0.52(1)
P ₄	0.52(2)	0.500(2)	0.511(1)	0.505(9)

ing that the line is in a disordered phase. Using the FSS $G_x \sim L^{-1/4}$ of a BKT transition [inset of Fig. 3(a)], we find a transition point at K_1 . We then analyze the correlation length $\xi_x = (2\sin\frac{\pi}{L})^{-1} \sqrt{\frac{\langle M_x^2 \rangle}{\langle M_{xk}^2 \rangle}} - 1$ of the x line with $M_x = L^{-1} |\sum_{\mathbf{r} \in \text{an } x \text{ line}} \vec{S}_r|$ and $M_{xk} = L^{-1} |\sum_{\mathbf{r} \in \text{an } x \text{ line}} \vec{S}_r e^{i\frac{2\pi}{L}x}|$. Figure 3(b) shows that ξ_x/L starts to be scale-invariant at K_1 . Figure 3(c) demonstrates that dG_x/dK is peaked at K_1 and decreases drastically at K_2 . For each L , we define the pseudo-critical points $K_1(L)$ and $K_2(L)$: $K_1(L)$ is the location of the peak of dG_x/dK , while $K_2(L)$ is the numerical result of K satisfying $dG_x/dK = 0.4$. For $K_1(L)$ and $K_2(L)$, we perform fits according to Eq. (3) separately. With $l_0 = 1$, we obtain $K_1 = 0.751(10)$ and $\chi^2/\text{DOF} \approx 0.4$ with $L_{\min} = 16$. For $K_2(L)$, with free l_0 , we obtain $K_2 = 1.12(8)$ with $L_{\min} = 16$. It is therefore confirmed that $K_2 = J_{\text{KBT}}$. An additional verification is that, the $L \rightarrow \infty$ limit of $K_1(L)$ extracted from $d(\xi_x/L)/dK$ goes to $K_1 = 0.75(3)$ with $\chi^2/\text{DOF} \approx 1.0$ and $L_{\min} = 64$, which is consistent with aforementioned estimates of K_1 . The variation of $K_n(L)$ with $[\ln(L/l_0)]^{-2}$ ($n = 1, 2$) is shown in Fig. 3(d). A good agreement is found between estimated K_n from y and x lines.

Summarizing, we find iterative transitions at K_1 and K_2 for $0 < W < J_{\text{KBT}}$. In the intermediate regime $K_1 < K < K_2$, the V plane is critical. For $W > J_{\text{KBT}}$, the V plane is already in a QLR ordered phase at $K = 0$. In SM, by increasing K , we confirm the existence of transition at K_2 . The transition lines for K_1 and K_2 can be found in Fig. 1.

Long-range Ordered Phase. For $K > K_2$, Fig. 2(b) implies that ξ_y/L grows rapidly with L , indicating the possibility of LR order along y direction. In what follows, for y and x lines, we explore ordering by using four parameter sets P₁: ($W = 0.8, K = 1.5$), P₂: ($W = 0.8, K = 2$), P₃: ($W = 1.5, K = 1.5$) and P₄: ($W = 1.5, K = 2$).

If the scenario is the LR order associated with the breaking of $O(2)$ symmetry, Goldstone mode probably plays a role and spin-spin correlation function scales as [40]

$$g(\Delta y) = a + b(\Delta y)^{-q} \quad (4)$$

with Δy the spatial distance, where q is an exponent controlling leading decay and b denotes a non-universal constant. Further, the value of q , arising from the Gaussian expansion of the transverse (Goldstone) mode around the LR spontaneous order m , is expected to be independent of couplings W and K , which only affect the magnitude of m . It follows that G_y

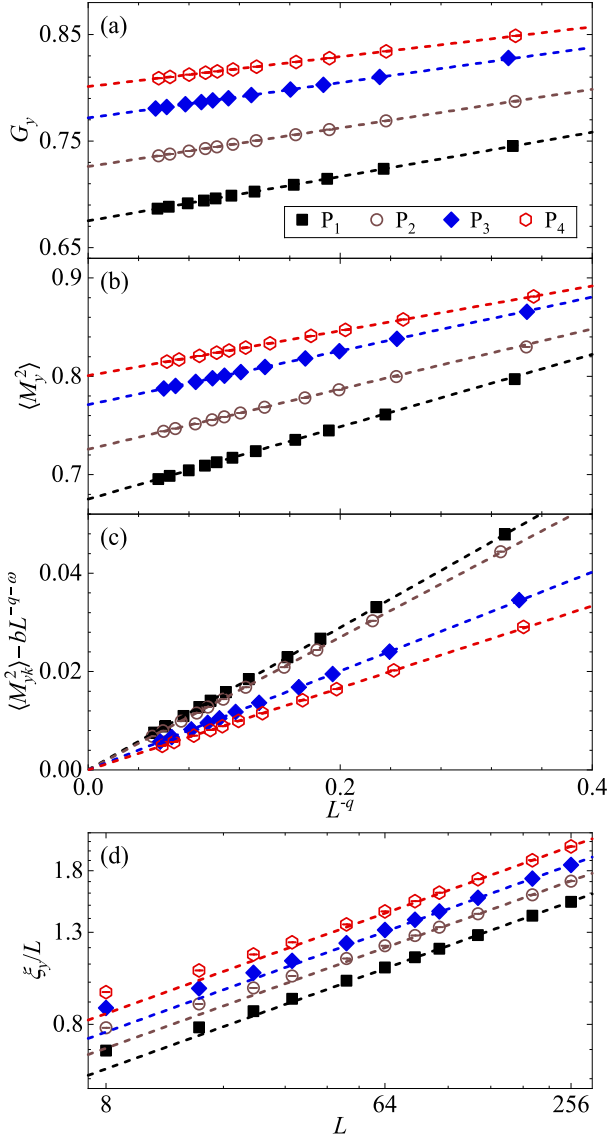


Figure 4. Goldstone-mode effects of the LR order of a y line in the V plane. (a)-(b) The large-distance spin-spin correlation G_y and the zero-mode magnetic fluctuations $\langle M_y^2 \rangle$ versus L^{-q} . The values of q are obtained from preferred fits (Table I). The intercepts stand for the values of G_y or $\langle M_y^2 \rangle$ in the thermodynamic limit. (c) The magnetic fluctuations at smallest non-zero mode (with finite-size corrections being considered), $\langle M_{yk}^2 \rangle - bL^{-q-\omega}$, versus L^{-q} . For P_1, P_2, P_3 and P_4 , the values $\omega = 0.62, 0.39, 1.1$ and 1.16 are from preferred fits, respectively. (d) Log-log plot of the reduced correlation length ξ_y/L versus L . The slope 0.255 of dashed lines stands for $q/2$.

and the magnetic fluctuations $\langle M_y^2 \rangle$ respectively obey the FSS formulae [6]

$$G_y = a + bL^{-q} \quad \text{and} \quad \langle M_y^2 \rangle = a + bL^{-q}. \quad (5)$$

The non-universal constant a now represents the value of G_y or $\langle M_y^2 \rangle$ in the thermodynamic limit. By performing fits of G_y according to Eq. (5), we obtain $q = 0.523(1), 0.5204(8), 0.528(2)$ and $0.52(2)$ as well as $\chi^2/\text{DOF} \approx 1.0, 1.2, 1.1$

and 1.0 , with $L_{\min} = 24, 16, 24$ and 96 , for P_1, P_2, P_3 and P_4 , respectively. From $\langle M_y^2 \rangle$, we obtain $q = 0.521(4), 0.508(4), 0.5074(8)$ and $0.500(2)$ as well as $\chi^2/\text{DOF} \approx 1.3, 0.8, 0.8$ and 1.0 , with $L_{\min} = 80, 80, 32$ and 64 , for P_1, P_2, P_3 and P_4 , respectively. The FSS behaviors of G_y and $\langle M_y^2 \rangle$ [Figs. 4(a) and (b)], particularly their non-zero thermodynamic limits, provide strong evidence of LR order. According to Eq. (4), we further predict that constant contribution is vanishing in the magnetic fluctuations $\langle M_{yk}^2 \rangle$ at smallest non-zero mode, which scales as [6]

$$\langle M_{yk}^2 \rangle = L^{-q}(a + bL^{-\omega}), \quad (6)$$

where ω is a correction exponent. By performing fits, we obtain $q = 0.5321(10), 0.537(7), 0.516(2)$ and $0.511(1)$ as well as $\chi^2/\text{DOF} \approx 1.1, 2.3, 0.3$ and 1.4 , with $L_{\min} = 8, 24, 24$ and 24 , for P_1, P_2, P_3 and P_4 , respectively. With finite-size corrections being handled, the linear dependence of $\langle M_{yk}^2 \rangle$ on L^{-q} is shown in Fig. 4(c).

We explain the FSS behaviors of ξ_y/L for $K > K_2$. According to the definition of ξ_y , an asymptotic relation reads $(\xi_y/L)^2 \sim \langle M_y^2 \rangle / \langle M_{yk}^2 \rangle$. Using Eqs. (5) and (6), the scaling formula of $(\xi_y/L)^2$ is written as [6]

$$(\xi_y/L)^2 = L^q(a + bL^{-\omega}) + c, \quad (7)$$

with c a background term. By fits, we obtain $q = 0.533(2), 0.52(1), 0.52(1)$ and $0.505(9)$ as well as $\chi^2/\text{DOF} \approx 0.3, 1.7, 0.3$ and 1.5 , with $L_{\min} = 8, 16, 24$ and 16 , for P_1, P_2, P_3 and P_4 , respectively. The power-law divergence of ξ_y/L upon increasing L , shown in Fig. 4(d), is therefore related to the LR order.

The values of q extracted from different parameter sets are close to each other (Table I). Such a universality provides further evidence of Goldstone-mode effects. A final estimate of q is $q = 0.51(2)$, which might be exactly identical to $1/2$ and remains to be theoretically derived.

A distinct scenario is observed for the x lines. Figure 3(b) implies that, for $K > K_2$, ξ_x/L does not diverge with increasing L . Figure 5(a) shows that, ξ_x/L converges in the thermodynamic limit. The size-dependent behavior of ξ_x/L can be quantified by extrapolation to constant supplemented by logarithmic or power-law finite-size corrections (SM). Moreover, we find that the finite-size corrections are largely suppressed if a slightly different definition of correlation length is utilized.

This definition reads $\xi'_x = (2\sin\frac{\pi}{L})^{-1} \sqrt{\frac{\Gamma_V(0,0)}{\Gamma_V(\frac{2\pi}{L},0)}} - 1$, with $\Gamma_V(\mathbf{k}) = L^{-4} \langle |\sum_{\mathbf{r} \in V} \vec{S}_{\mathbf{r}} e^{i\mathbf{k} \cdot \mathbf{r}}|^2 \rangle$, where the summation runs over sites in the V plane. Figure 5(a) demonstrates that ξ'_x/L converges fast to constant as $L \rightarrow \infty$. The existence of critical phase is confirmed. Furthermore, we find that G_x can be described by

$$G_x = a[\ln(L/l_0)]^{-\hat{q}}, \quad (8)$$

with \hat{q} a critical exponent. By fits, we obtain $\hat{q} = 0.049(2), 0.039(8), 0.035(3)$ and $0.026(2)$ as well as $\chi^2/\text{DOF} \approx 0.8, 0.7, 1.9$ and 1.3 , with $L_{\min} = 48, 80, 64$ and 64 , for P_1, P_2, P_3 and P_4 , respectively. The dependence of G_x on $\ln(L/l_0)$

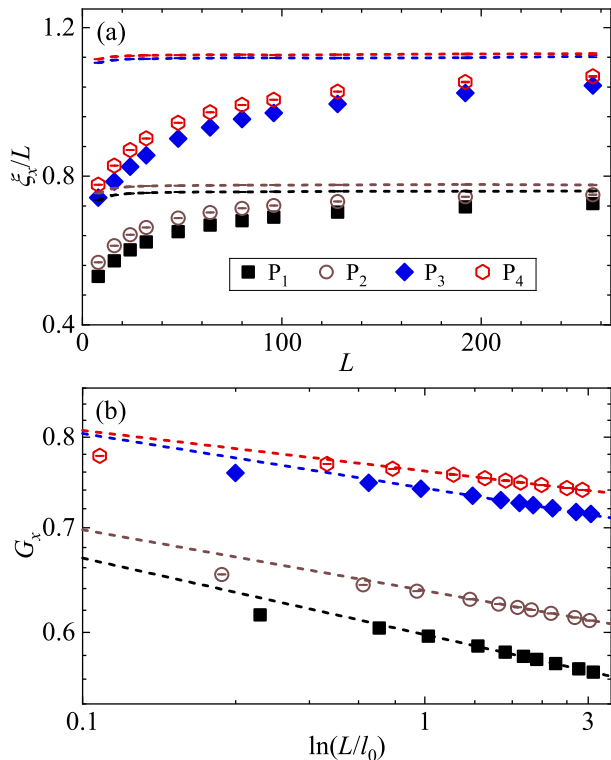


Figure 5. Critical phase of an x line in the V plane. (a) Reduced correlation length ξ_x/L versus L . The dashed lines represent ξ'_x/L . (b) Log-log plot of the large-distance spin-spin correlation G_x versus $\ln(L/l_0)$. The dashed lines represent preferred fits according to Eq. (8). For P_1 , P_2 , P_3 and P_4 , the values $l_0 = 11.5, 12.4, 12.1$ and 14.3 are from preferred fits, respectively.

is illustrated by Fig. 5(b). It is of practical difficulty to completely preclude the power-law scaling $G_x \sim L^{-\tilde{q}}$ with \tilde{q} a critical exponent, though the possibility is small (SM). Finally, we point out that, albeit the logarithmic scenario possibly exists, it differs from the E-Log scenario of surface and interface criticality, where the correlation length diverges logarithmically with L [13] owing to the two-length scaling of correlation function [14].

In short, when $W > 0$ and $K > K_2$, the y lines enter a LR

ordered phase, whereas a critical phase emerges in the x lines. Hence, the ordering in the V plane is anisotropic. An intuitive picture for such anisotropy is that the ordering along y (resp. x) lines is directly (resp. indirectly) enhanced by the effective interactions mediated by P planes.

Summary and Discussions. The exploration of LR order in a SR Q2D XY model is motivated jointly by the latest advances in the surface and interface critical phenomena, the rapid development of defect conformal field theory, as well as the novel concept QTF. By proposing a new setup, we provide the first piece of conclusive evidence that LR order emerges in a Q2D XY model with finite SR couplings. Employing a comprehensive scaling analysis, we unveil that the LR ordered phase exhibits Goldstone-mode physics. Our findings largely expand the current understanding of the low-dimensional XY model associated with superfluidity.

Albeit our setup could be seen as an isotropic generalization of comb lattice to the 3D case, the current LR order is drastically different from the crucial features of QTF. First, our observations are free from quantum-mechanical effects. Second, QTF corresponds to the LR order along the x direction of our setup, whereas LR order is now found along the y lines.

The present study will be generalized to various contexts. First, our setup can be utilized to study various classical and quantum critical systems, such as the Ising, XY and Heisenberg systems. In each situation, it is interesting to examine whether (if so, how) the ordering of the V plane can be made strengthened. Second, our results imply that, it is worthwhile to study the impurity problems of the quantum Bose-Hubbard model on the 2D comb lattice. Finally, it is promising to realize the LR order of cold atoms with controlled emulation using optical lattices. We leave these outstanding problems to future studies.

Acknowledgments. M.H., C.Z., D.Z., Y.S. and J.-P.L. are supported by the National Natural Science Foundation of China under Grants No. 12275002 and 12204173. Y.D. is supported by the National Natural Science Foundation of China under Grant No. 12275263, the Innovation Program for Quantum Science and Technology under Grant No. 2021ZD0301900, and the Natural Science Foundation of Fujian Province of China under Grant No. 2023J02032.

-
- [1] J. M. Kosterlitz, Nobel lecture: Topological defects and phase transitions, *Rev. Mod. Phys.* **89**, 040501 (2017).
 - [2] H. Kunz and C. E. Pfister, First order phase transition in the plane rotator ferromagnetic model in two dimensions, *Comm. Math. Phys.* **46**, 245 (1976).
 - [3] G. Giachetti, N. Defenu, S. Ruffo, and A. Trombettoni, Berezinskii-kosterlitz-thouless phase transitions with long-range couplings, *Phys. Rev. Lett.* **127**, 156801 (2021), [arXiv:2104.13217 \[cond-mat\]](https://arxiv.org/abs/2104.13217).
 - [4] G. Giachetti, A. Trombettoni, S. Ruffo, and N. Defenu, Berezinskii-kosterlitz-thouless transitions in classical and quantum long-range systems, *Phys. Rev. B* **106**, 014106 (2022), [arXiv:2201.03650 \[cond-mat\]](https://arxiv.org/abs/2201.03650).
 - [5] T. Xiao, D. Yao, C. Zhang, Z. Fan, and Y. Deng, Two-dimensional xy ferromagnet induced by long-range interaction, [arXiv:2404.08498 \[cond-mat\]](https://arxiv.org/abs/2404.08498).
 - [6] D. Yao, T. Xiao, C. Zhang, Y. Deng, and Z. Fan, The non-classical regime of the two-dimensional long-range xy model: a comprehensive monte carlo study, [arXiv:2411.01811 \[cond-mat\]](https://arxiv.org/abs/2411.01811).
 - [7] L. Bianchi and D. Bonomi, Conformal dispersion relations for defects and boundaries, *SciPost Phys.* **15**, 055 (2023), [arXiv:2205.09775 \[hep-th\]](https://arxiv.org/abs/2205.09775).
 - [8] M. Trépanier, Surface defects in the o(n) model, *J. High Energy Phys.* **2023** (9), 74, [arXiv:2305.10486 \[hep-th\]](https://arxiv.org/abs/2305.10486).
 - [9] A. Raviv-Moshe and S. Zhong, Phases of surface defects

- in scalar field theories, *J. High Energ. Phys.* **2023**, 143, [arXiv:2305.11370 \[hep-th\]](#).
- [10] S. Giombi and B. Liu, Notes on a surface defect in the $o(n)$ model, *J. High Energ. Phys.* **2023**, 4, [arXiv:2305.11402 \[hep-th\]](#).
- [11] I. C. Bolla, D. Rodriguez-Gomez, and J. G. Russo, Defects, rigid holography, and c -theorems, *Phys. Rev. D* **108**, L041701 (2023), [arXiv:2306.11796 \[hep-th\]](#).
- [12] G. Cuomo and S. Zhang, Spontaneous symmetry breaking on surface defects, *J. High Energ. Phys.* **2024**, 22, [arXiv:2306.00085 \[hep-th\]](#).
- [13] M. A. Metlitski, Boundary criticality of the $O(N)$ model in $d = 3$ critically revisited, *SciPost Phys.* **12**, 131 (2022), [arXiv:2009.05119 \[cond-mat\]](#).
- [14] M. Hu, Y. Deng, and J.-P. Lv, Extraordinary-log surface phase transition in the three-dimensional xy model, *Phys. Rev. Lett.* **127**, 120603 (2021), [arXiv:2104.05152 \[cond-mat\]](#).
- [15] F. Parisen Toldin and M. A. Metlitski, Boundary criticality of the 3d $o(n)$ model: from normal to extraordinary, *Phys. Rev. Lett.* **128**, 215701 (2022), [arXiv:2111.03613 \[cond-mat\]](#).
- [16] A. Krishnan and M. A. Metlitski, A plane defect in the 3d $O(N)$ model, *SciPost Phys.* **15**, 090 (2023), [arXiv:2301.05728 \[cond-mat\]](#).
- [17] Y. Sun, M. Hu, Y. Deng, and J.-P. Lv, Extraordinary-log universality of critical phenomena in plane defects, *Phys. Rev. Lett.* **131**, 207101 (2023), [arXiv:2301.11720 \[cond-mat\]](#).
- [18] F. Parisen Toldin, Boundary critical behavior of the three-dimensional heisenberg universality class, *Phys. Rev. Lett.* **126**, 135701 (2021), [arXiv:2012.00039 \[cond-mat\]](#).
- [19] L.-R. Zhang, C. Ding, Y. Deng, and L. Zhang, Surface criticality of the antiferromagnetic potts model, *Phys. Rev. B* **105**, 224415 (2022), [arXiv:2204.11692 \[cond-mat\]](#).
- [20] X. Zou, S. Liu, and W. Guo, Surface critical properties of the three-dimensional clock model, *Phys. Rev. B* **106**, 064420 (2022), [arXiv:2204.13612 \[cond-mat\]](#).
- [21] Y. Sun and J.-P. Lv, Quantum extraordinary-log universality of boundary critical behavior, *Phys. Rev. B* **106**, 224502 (2022), [arXiv:2205.00878 \[cond-mat\]](#).
- [22] Y. Sun, J. Lyu, and J.-P. Lv, Classical-quantum correspondence of special and extraordinary-log criticality: Villain's bridge, *Phys. Rev. B* **106**, 174516 (2022), [arXiv:2211.11376 \[cond-mat\]](#).
- [23] L. R. Zhang, C. Ding, W. Zhang, and L. Zhang, Sublattice extraordinary-log phase and new special point of the antiferromagnetic potts model, *Phys. Rev. B* **108**, 024402 (2023), [arXiv:2301.08926 \[cond-mat\]](#).
- [24] J. Y. Lee, C.-M. Jian, and C. Xu, Quantum criticality under decoherence or weak measurement, *PRX Quantum* **4**, 030317 (2023), [arXiv:2301.05238 \[cond-mat\]](#).
- [25] K. Baweja, D. J. Luitz, and S. J. Garratt, Post-measurement quantum monte carlo, [arXiv:2410.13844 \[cond-mat\]](#).
- [26] Y.-H. Zhang, Z. Zhu, and A. Vishwanath, Xy^* transition and extraordinary boundary criticality from fractional exciton condensation in quantum hall bilayer, *Phys. Rev. X* **13**, 031023 (2023), [arXiv:2302.03703 \[cond-mat\]](#).
- [27] X. Sun and S.-K. Jian, Boundary operator expansion and extraordinary phase transition in the tricritical $o(n)$ model, [arXiv:2501.06287 \[cond-mat\]](#).
- [28] X. Sun and S.-K. Jian, Boundary operator expansion and extraordinary-log phase in the tricritical $o(n)$ model, *APS Global Physics Summit* (2025).
- [29] L. Radzihovsky, A. Kuklov, N. Prokof'ev, and B. Svistunov, Superfluid edge dislocation: Transverse quantum fluid, *Phys. Rev. Lett.* **131**, 196001 (2023), [arXiv:2304.03309 \[cond-mat\]](#).
- [30] A. Kuklov, N. Prokof'ev, L. Radzihovsky, and B. Svistunov, Transverse quantum fluids, *Phys. Rev. B* **109**, L100502 (2024), [arXiv:2309.02501 \[cond-mat\]](#).
- [31] A. Kuklov, L. Pollet, N. Prokof'ev, L. Radzihovsky, and B. Svistunov, Universal correlations as fingerprints of transverse quantum fluids, *Phys. Rev. A* **109**, L011302 (2024), [arXiv:2310.19875 \[cond-mat\]](#).
- [32] L. Radzihovsky and E. Pellett, Quantum phases and transitions of bosons on a comb lattice, [arXiv:2412.06915 \[cond-mat\]](#).
- [33] A. Kuklov, L. Pollet, N. Prokof'ev, and B. Svistunov, Transverse quantum superfluids, *Annu. Rev. Condens. Matter Phys.* **16** (2024), [arXiv:2404.15480 \[cond-mat\]](#).
- [34] C. Zhang, M. Boninsegni, A. Kuklov, N. Prokof'ev, and B. Svistunov, Superclimbing modes in transverse quantum fluids: Signature statistical and dynamical features, *Phys. Rev. B* **109**, 214519 (2024), [arXiv:2404.03465 \[cond-mat\]](#).
- [35] A. Kuklov, N. Prokof'ev, and B. Svistunov, Autonomous dynamics of two-dimensional insulating domain with superclimbing edges, *Phys. Rev. Res.* **6**, 033008 (2024), [arXiv:2404.18290 \[cond-mat\]](#).
- [36] Y. Komura and Y. Okabe, Large-scale monte carlo simulation of two-dimensional classical xy model using multiple gpus, *J. Phys. Soc. Jpn.* **81**, 113001 (2012), [arXiv:1210.6116 \[cond-mat\]](#).
- [37] U. Wolff, Collective monte carlo updating for spin systems, *Phys. Rev. Lett.* **62**, 361 (1989).
- [38] J. M. Kosterlitz, The critical properties of the two-dimensional xy model, *J. Phys. C* **7**, 1046 (1974).
- [39] Y. Tomita and Y. Okabe, Probability-changing cluster algorithm for two-dimensional XY and clock models, *Phys. Rev. B* **65**, 184405 (2002), [arXiv:cond-mat/0202161 \[cond-mat\]](#).
- [40] M. Kardar, *Statistical physics of fields* (Cambridge University Press, 2007).

Supplemental Material for “Long-range Order in a Short-range Quasi-2D XY Model”

I. MONTE CARLO SIMULATIONS

The Wolff’s cluster algorithm is employed to perform Monte Carlo simulations. In each Markov chain simulation, the first one sixth of Monte Carlo steps are used for thermalization, while samplings are performed after a constant number n_c of Wolff clusters are created. Hence, correlations between sampled configurations are suppressed. When W and L are specified, the value of n_c is generally set to decrease with increasing K . For $W = 0.8$ and 1.5 , the ranges of cluster numbers are summarized in Table I.

II. PHASE TRANSITIONS WITH $W = 0.8$

To quantify the variation of ξ_y/L with K , we compute the derivative $d(\xi_y/L)/dK$. To this end, we first apply a linear method to perform interpolation of ξ_y/L , and then employ a differential module without any smoothing. Such a procedure is utilized to obtain all numerical differentials throughout this Letter. When L is sufficiently large, we find a pair of peaks $K_1(L)$ and $K_2(L)$ [$K_1(L) < K_2(L)$] from the $d(\xi_y/L)/dK$ - K curve and a peak $K_1(L)$ from the dG_y/dK - K curve. Note that the measurement errors of $K_1(L)$ and $K_2(L)$ are not statistical. For $K_1(L)$, we perform least-squares fits according to the scaling formula

$$K_n(L) = K_n + a[\ln(L/l_0)]^{-2} \quad (1)$$

with $n = 1$, where a denotes a non-universal constant and l_0 represents a reference length. Similarly, we estimate K_2 according to Eq. (1) with $n = 2$. The results of fits are summarized in Table II.

We consider an x line. Similar to what has done for the y line, we perform least-squares fits of $K_1(L)$, extracted from dG_x/dK and $d(\xi_x/L)/dK$, according to Eq. (1). We also perform fits of $K_2(L)$, which, for each L , is now a value of K satisfying $dG_x/dK = 0.4$. Details of fits are given in Table II.

III. PHASE TRANSITIONS WITH $W = 1.5$

From Figs. 1(a) and (b), we infer a singularity at K_2 from G_y and ξ_y/L , respectively. This result indicates a phase transition at K_2 for a y line. Figure 1(c) shows that, for each L , the derivative $d(\xi_y/L)/dK$ is peaked at $K_2(L)$. We perform fits of $K_2(L)$ according to Eq. (1), which yield $K_2 = 1.2(2)$ and $\chi^2/\text{DOF} \approx 0.3$ with $L_{\min} = 32$. The estimate of K_2 is consistent with $K_2 \approx 1.11996$. By fixing $K_2 = 1.11996$, we obtain $l_0 = 0.2(1)$ and $\chi^2/\text{DOF} \approx 0.2$ with $L_{\min} = 32$. Details of fits are presented in Table III. The dependence of $K_2(L)$ on $[\ln(L/l_0)]^{-2}$ is illustrated in Fig. 1(d).

For an x line, we observe that G_x exhibits a kink at K_2 [Fig. 2(a)]. For $K > K_2$, Fig. 2(b) implies that ξ_x/L con-

Table I. The range of Wolff cluster numbers with $W = 0.8$ and 1.5 . n_{\min} and n_{\max} denote the minimum and maximum numbers, respectively. “-” implies $n_{\max} = n_{\min}$.

L	n_{\min}	n_{\max}
8	2.9×10^8	-
16	5.8×10^8	-
24	8.6×10^8	-
32	1.2×10^9	3.5×10^{10}
48	2.2×10^8	-
64	2.2×10^8	2.8×10^{10}
80	7.2×10^7	-
96	7.2×10^7	-
128	1.4×10^7	4.6×10^9
192	7.2×10^6	-
256	3.6×10^6	3.1×10^8

verges roughly as $L \rightarrow \infty$, indicating the possibility of a critical phase. The sharp reduction in dG_x/dK at K_2 provides complementary evidence of a phase transition [Fig. 2(c)]. For each L , $K_2(L)$ is defined with $dG_x/dK = 0.2$. We fit $K_2(L)$ to Eq. (1) and obtain $K_2 = 1.13(7)$ with $L_{\min} = 32$. The estimate of K_2 again agrees well with $K_2 \approx 1.11996$. Details of fits are given in Table III. The dependence of $K_2(L)$ on $[\ln(L/l_0)]^{-2}$ is shown in Fig. 2(d).

IV. THE PHASES AT $K > K_2$

A. y lines

As discussed in the main text, the y lines may enter a LR ordered phase with $K > K_2$, which can be related to the Goldstone mode. It follows that the large-distance spin-spin correlation G_y , the magnetic fluctuations $\langle M_y^2 \rangle$ at zero mode, the magnetic fluctuations $\langle M_{yk}^2 \rangle$ at smallest non-zero mode and the correlation length ξ_y obey the FSS formulae

$$G_y = a + bL^{-q}, \quad (2)$$

$$\langle M_y^2 \rangle = a + bL^{-q}, \quad (3)$$

$$\langle M_{yk}^2 \rangle = L^{-q}(a + bL^{-\omega}) \quad (4)$$

and

$$(\xi_y/L)^2 = L^q(a + bL^{-\omega}) + c \quad (5)$$

respectively, where the exponent q controls the leading FSS behavior, ω is a correction exponent, while a , b and c are non-universal constants. We fit the Monte Carlo data of G_y , $\langle M_y^2 \rangle$,

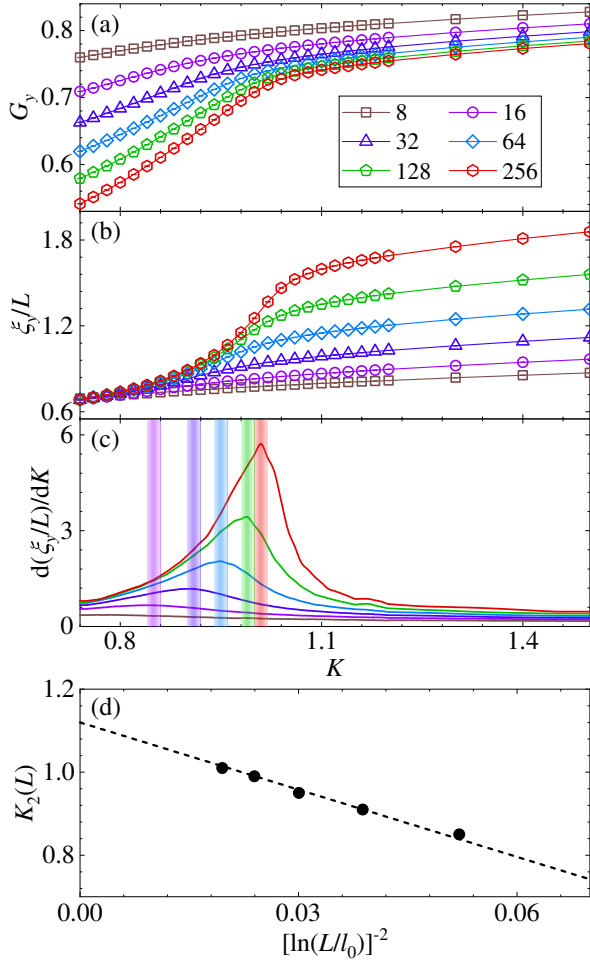


Figure 1. Quantities of a y line in the V plane with $W = 1.5$. (a) The large-distance spin-spin correlation G_y versus K . (b) The reduced correlation length ξ_y/L versus K . (c) The derivative $d(\xi_y/L)/dK$ versus K . The shadowed areas, whose widths represent two error bars, denote $K_2(L)$ (the K coordinate of the peak). (d) $K_2(L)$ from $d(\xi_y/L)/dK$ versus $[\ln(L/l_0)]^{-2}$, where $l_0 = 0.2$ comes from a preferred fit. The intercept $K_2 = 1.11996$ represents the thermodynamic limit of $K_2(L)$.

$\langle M_{y_k}^2 \rangle$ and ξ_y to Eqs. (2), (3), (4) and (5), respectively. The results are given in Tables IV, V, VI and VII.

Having confirmed scaling formulae (3) and (4), we analyze the residual magnetic fluctuations $R = \langle M_y^2 \rangle - f \langle M_{y_k}^2 \rangle$, where the parameter f is set, according to Eqs. (3) and (4), to cancel the term with L^{-q} . Therefore, R features reduced finite-size corrections and obeys

$$R = a + bL^{-\omega}. \quad (6)$$

Using Eq. (6), we obtain $a = 0.67556(9)$, $0.72676(5)$, $0.77175(3)$ and $0.8011(1)$ as well as $\chi^2/\text{DOF} \approx 0.7$, 1.5 , 0.7 and 0.8 , with $L_{\min} = 48$, 32 , 32 and 64 , for P_1 , P_2 , P_3 and P_4 , respectively. Details of fits are given in Table VIII. Figure 3(a) displays R versus $L^{-\omega}$. Indeed, if compared to $\langle M_y^2 \rangle$ (main text), R converges faster as L increases.

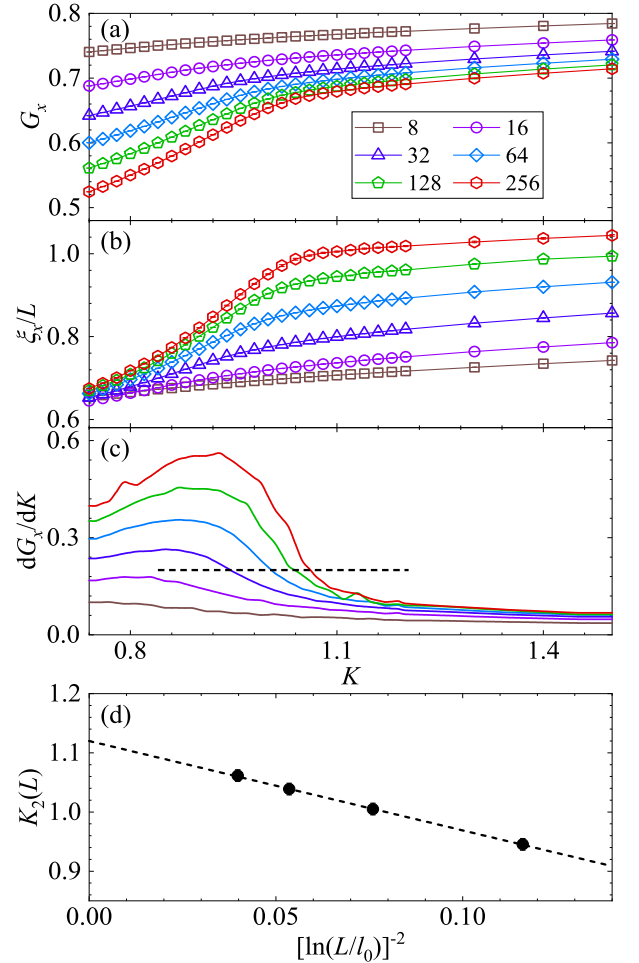


Figure 2. Quantities of an x line in the V plane with $W = 1.5$. (a) (b) Same as Figs. 1(a) and (b) but for the x line. (c) The derivative dG_x/dK versus K . The dashed line represents $dG_x/dK = 0.2$. (d) $K_2(L)$ from dG_x/dK versus $[\ln(L/l_0)]^{-2}$, where $l_0 = 1.7$ comes from a preferred fit. The intercept $K_2 = 1.11996$ represents the thermodynamic limit of $K_2(L)$.

Finally, we provide additional evidence of LR ordered phase by using an alternative definition of correlation length, namely $\xi'_y = (2 \sin \frac{\pi}{L})^{-1} \sqrt{\frac{\Gamma_V(0,0)}{\Gamma_V(0, \frac{2\pi}{L})}} - 1$. The power-law dependence of ξ'_y/L with L is indicated by Fig. 3(b). By fitting ξ'_y/L to

$$\xi'_y/L = aL^{q'} + b, \quad (7)$$

we obtain $q' = 0.516(6)$, $0.50(1)$, $0.514(2)$ and $0.504(2)$ as well as $\chi^2/\text{DOF} \approx 1.1$, 0.9 , 1.7 and 2.5 , with $L_{\min} = 64$, 80 , 24 and 24 , for P_1 , P_2 , P_3 and P_4 , respectively. It is found that, for P_1 , P_2 , P_3 and P_4 , the estimates of q' are close to each other. Details of fits are given in Table IX.

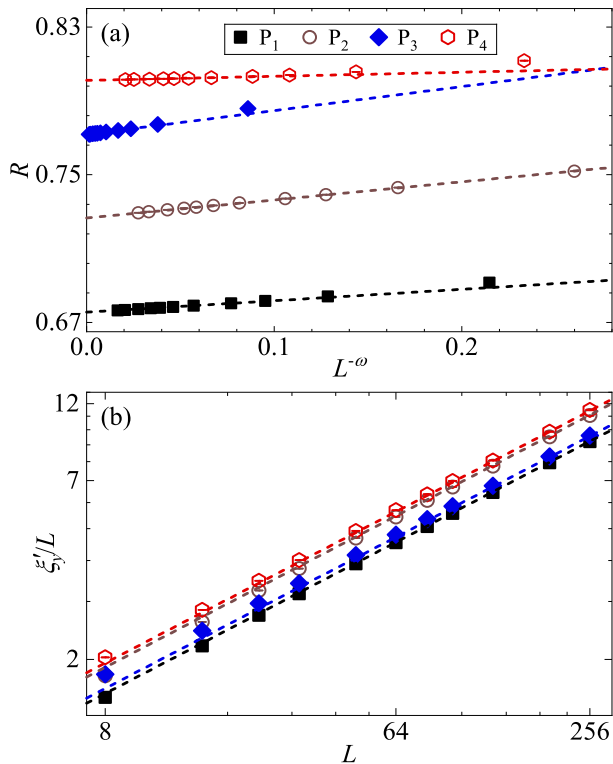


Figure 3. Additional quantities for the LR ordered phase of a y line in the V plane. (a) The residual magnetic fluctuations R versus $L^{-\omega}$. For P_1 , P_2 , P_3 and P_4 , the values $\omega = 0.74, 0.648, 1.18$ and 0.7 are from preferred fits, respectively. (b) Log-log plot of the reduced correlation length ξ'_y/L versus L . The slope 0.51 of dashed lines stands for q' .

B. x lines

Assuming the x lines are critical, we fit ξ_x/L to the scaling formula

$$\xi_x/L = a + bL^{-\omega}, \quad (8)$$

where a represents the non-zero value of ξ_x/L in the thermodynamic limit and $bL^{-\omega}$ is a power-law correction term. We obtain $a = 0.770(8), 0.788(9), 1.24(2)$ and $1.19(1)$ as well as $\chi^2/\text{DOF} \approx 0.3, 1.0, 1.2$ and 1.0 , with $L_{\min} = 80, 80, 48$ and 48 , for P_1, P_2, P_3 and P_4 , respectively. The results are summarized in Table X. We also fit ξ_x/L to the formula

$$\xi_x/L = a + b(\ln L)^{-\omega}, \quad (9)$$

with $b(\ln L)^{-\omega}$ a logarithmic correction term. We obtain $a = 0.80(2), 0.82(1), 1.5(1)$ and $1.43(5)$ as well as $\chi^2/\text{DOF} \approx 0.4, 0.8, 0.3$ and 1.1 , with $L_{\min} = 80, 64, 64$ and 48 , for P_1, P_2, P_3 and P_4 , respectively. The results are summarized in Table XI. Hence, it is practically difficult to differentiate scaling formulae (8) and (9). However, both formulae imply that ξ_x/L is finite in the thermodynamic limit.

The large-distance spin-spin correlation G_x is fitted according to the logarithmic FSS formula

$$G_x = a[\ln(L/l_0)]^{-\tilde{q}}, \quad (10)$$

with \tilde{q} a critical exponent. The results are presented in Table XII. We also perform fits according to the power-law FSS formula

$$G_x = aL^{-\tilde{q}} \quad (11)$$

with \tilde{q} a critical exponent, but find that χ^2/DOF is generally huge. The details are given in Table XIII.

V. THE P PLANES

It is inferred that the P planes experience a BKT transition at $K = J_{\text{BKT}}$ independent of W , which separates a disordered phase from the QLR ordered phase. To verify this point, for a P plane, we sample the magnetic fluctuations $\langle M_P^2 \rangle$ with $M_P = L^{-2} |\sum_{r \in P} \vec{S}_r|$, where the summation runs over sites in the P plane. For $W = 1.5$, using the scaling form $\langle M_P^2 \rangle \sim L^{-1/4}$, we confirm the existence of the BKT transition [Fig. 4(a)].

Furthermore, Fig. 4(b) illustrates that the Monte Carlo data of $\langle M_P^2 \rangle$ at $W = 0.8$ and 1.5 become more indistinguishable as L increases. This observation is consistent with the expectation that all quantities of a P plane are independent of W in the $L \rightarrow \infty$ limit.

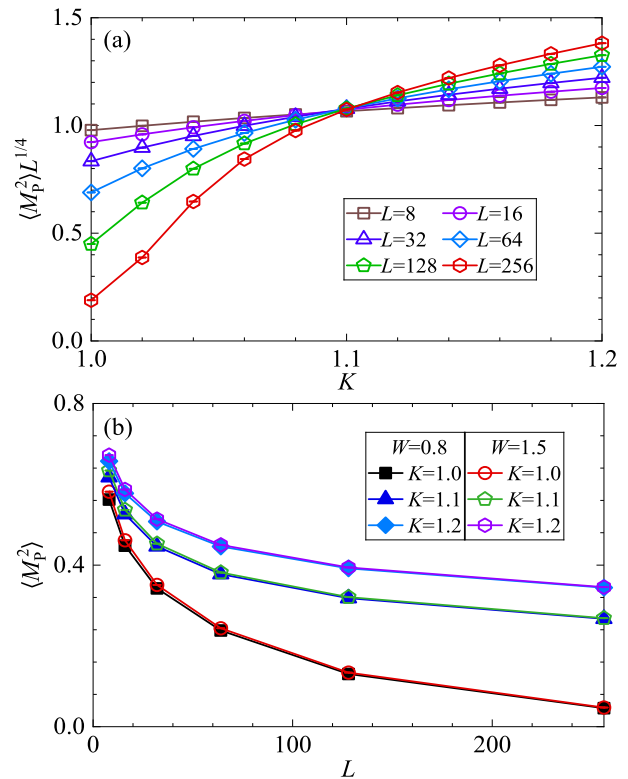


Figure 4. Analyses of magnetic fluctuations $\langle M_P^2 \rangle$ for a P plane. (a) The scaled magnetic fluctuations $\langle M_P^2 \rangle L^{1/4}$ versus K at $W = 1.5$. (b) $\langle M_P^2 \rangle$ versus L for different W and K .

Table II. Fits of $K_n(L)$ ($n = 1, 2$) to Eq. (1) for y and x lines with $W = 0.8$.

Quantity	n	L_{\min}	χ^2/DOF	K_n	a	l_0
$d(\xi_y/L)/dK$	1	32	0.97/2	0.75(1)	-0.7(3)	1
		64	0.97/1	0.75(3)	-0.7(6)	1
dG_y/dK	1	16	3.05/3	0.750(10)	-0.8(1)	1
		32	1.53/2	0.76(1)	-1.1(3)	1
		64	0.97/1	0.75(3)	-0.7(6)	1
		128	0.97/1	0.75(3)	-0.7(6)	1
$d(\xi_y/L)/dK$	2	16	0.14/2	1.07(2)	-1.4(7)	1.9(9)
		32	0.08/1	1.08(7)	-2.1(35)	1.2(26)
		16	2.78/3	1.11996	-3.3(4)	0.8(2)
		32	0.26/2	1.11996	-4.5(11)	0.4(2)
		64	0.17/1	1.11996	-5.1(25)	0.3(4)
		16	2.80/4	1.11996	-3.28(7)	0.8
		32	2.44/3	1.11996	-3.24(10)	0.8
		64	1.06/2	1.11996	-3.4(1)	0.8
		128	0.55/1	1.11996	-3.5(2)	0.8
		dG_x/dK	1	16	1.15/3	0.751(10)
32	0.41/2			0.76(1)	-0.9(3)	1
64	0.41/1			0.76(3)	-0.8(6)	1
$d(\xi_x/L)/dK$	1	32	0.97/2	0.75(1)	-0.7(3)	1
		64	0.97/1	0.75(3)	-0.7(6)	1
dG_x/dK	2	16	0.00/2	1.12(8)	-4.6(84)	0.1(4)
		32	0.00/1	1.1(2)	-4.4(193)	0.1(11)
		16	0.00/3	1.11996	-4.4(11)	0.13(9)
		32	0.00/2	1.11996	-4.3(18)	0.1(2)
		64	0.00/1	1.11996	-4.2(33)	0.1(4)
		16	0.00/4	1.11996	-4.3(2)	0.13
		32	0.00/3	1.11996	-4.3(2)	0.13
		64	0.00/2	1.11996	-4.3(3)	0.13
128	0.00/1	1.11996	-4.3(4)	0.13		

Table III. Fits of $K_2(L)$ to Eq. (1) for y and x lines with $W = 1.5$.

Quantity	L_{\min}	χ^2/DOF	K_2	a	l_0
$d(\xi_y/L)/dK$	16	0.28/2	1.2(1)	-11.4(168)	0.0(1)
	32	0.28/1	1.2(2)	-10.9(365)	0.0(3)
	16	0.45/3	1.11996	-6.6(11)	0.12(6)
	32	0.32/2	1.11996	-6.0(17)	0.2(1)
	64	0.17/1	1.11996	-5.1(25)	0.3(4)
	16	1.96/4	1.11996	-5.4(1)	0.2
	32	0.44/3	1.11996	-5.5(2)	0.2
	64	0.20/2	1.11996	-5.6(2)	0.2
	128	0.09/1	1.11996	-5.5(3)	0.2
	dG_x/dK	32	0.00/1	1.13(7)	-1.9(33)
32		0.03/2	1.11996	-1.5(4)	1.7(8)
64		0.01/1	1.11996	-1.4(8)	1.9(20)
32		0.03/3	1.11996	-1.51(6)	1.7
64		0.03/2	1.11996	-1.51(10)	1.7
128		0.02/1	1.11996	-1.5(1)	1.7

Table IV. Fits of G_y to Eq. (2) for a y line in the LR ordered phase.

Parameters	L_{\min}	χ^2/DOF	a	b	q
P ₁	8	23.20/8	0.67534(3)	0.2101(2)	0.5278(5)
	16	16.61/7	0.67526(5)	0.2094(3)	0.5262(8)
	24	6.06/6	0.67511(6)	0.2080(5)	0.523(1)
	32	5.91/5	0.67513(8)	0.2082(8)	0.523(2)
	48	5.19/4	0.6750(1)	0.207(2)	0.521(4)
	64	5.18/3	0.6750(2)	0.207(4)	0.521(6)
	80	1.78/2	0.6756(4)	0.219(8)	0.54(1)
	96	0.74/1	0.6752(6)	0.21(1)	0.52(2)
P ₂	16	8.16/7	0.72612(4)	0.1814(3)	0.5204(8)
	24	8.02/6	0.72613(6)	0.1816(5)	0.521(1)
	32	7.76/5	0.72611(7)	0.1813(7)	0.520(2)
	48	5.42/4	0.7263(1)	0.184(2)	0.525(4)
	64	0.76/3	0.7260(2)	0.178(3)	0.515(6)
	80	0.74/2	0.7259(3)	0.178(6)	0.51(1)
	96	0.66/1	0.7258(5)	0.175(10)	0.51(2)
	P ₃	16	40.85/7	0.77202(4)	0.1682(3)
24		6.75/6	0.77174(6)	0.1656(5)	0.528(2)
32		1.13/5	0.77161(9)	0.1641(8)	0.524(2)
48		0.27/4	0.7715(2)	0.162(2)	0.519(5)
64		0.27/3	0.7715(2)	0.162(4)	0.519(8)
80		0.03/2	0.7716(4)	0.165(8)	0.53(2)
96		0.02/1	0.7717(6)	0.17(1)	0.53(3)
P ₄		16	52.96/7	0.80153(4)	0.1414(2)
	24	30.38/6	0.80135(5)	0.1397(4)	0.523(2)
	32	8.04/5	0.80113(7)	0.1374(6)	0.516(2)
	48	7.73/4	0.8011(1)	0.137(2)	0.513(5)
	64	2.59/3	0.8007(2)	0.131(3)	0.499(8)
	80	2.56/2	0.8007(3)	0.131(5)	0.50(1)
	96	0.98/1	0.8012(5)	0.140(10)	0.52(2)

Table V. Fits of $\langle M_y^2 \rangle$ to Eq. (3) for a y line in the LR ordered phase.

Parameters	L_{\min}	χ^2/DOF	a	b	q
P ₁	24	48.15/6	0.67442(4)	0.3570(3)	0.5102(4)
	32	8.56/5	0.67462(5)	0.3591(4)	0.5127(6)
	48	6.26/4	0.67472(9)	0.361(1)	0.514(1)
	64	6.15/3	0.6748(1)	0.361(2)	0.515(2)
	80	2.63/2	0.6751(2)	0.368(4)	0.521(4)
	96	1.62/1	0.6748(3)	0.362(7)	0.516(6)
P ₂	32	22.21/5	0.72532(4)	0.2991(4)	0.5003(6)
	48	2.76/4	0.72559(7)	0.3026(9)	0.505(1)
	64	2.39/3	0.7256(1)	0.303(2)	0.506(2)
	80	1.61/2	0.7258(2)	0.306(3)	0.508(4)
	96	1.47/1	0.7258(3)	0.307(5)	0.510(6)
P ₃	24	11.66/6	0.77102(4)	0.2727(3)	0.5059(5)
	32	4.05/5	0.77112(5)	0.2736(4)	0.5074(8)
	48	0.63/4	0.77125(9)	0.275(1)	0.510(2)
	64	0.63/3	0.7713(1)	0.275(2)	0.510(3)
	80	0.42/2	0.7713(2)	0.277(4)	0.512(5)
	96	0.27/1	0.7712(3)	0.275(7)	0.509(8)
P ₄	16	63.55/7	0.80057(2)	0.2287(1)	0.4999(3)
	24	12.55/6	0.80074(3)	0.2300(2)	0.5027(5)
	32	9.48/5	0.80078(4)	0.2305(3)	0.5035(7)
	48	8.41/4	0.80084(7)	0.2313(8)	0.505(1)
	64	2.95/3	0.8007(1)	0.228(1)	0.500(2)
	80	2.31/2	0.8005(2)	0.226(3)	0.497(4)
	96	0.38/1	0.8008(3)	0.232(5)	0.505(7)

Table VI. Fits of $\langle M_{y_k}^2 \rangle$ to Eq. (4) for a y line in the LR ordered phase.

Parameters	L_{\min}	χ^2/DOF	q	a	b	ω
P ₁	8	7.86/7	0.5321(10)	0.1448(9)	-0.0692(3)	0.62(2)
	16	1.72/6	0.529(2)	0.141(1)	-0.073(2)	0.71(4)
	24	1.12/5	0.527(2)	0.140(2)	-0.078(7)	0.76(8)
	32	0.81/4	0.525(4)	0.138(3)	-0.09(3)	0.9(2)
	48	0.53/3	0.53(1)	0.14(1)	-0.06(3)	0.6(5)
P ₂	24	11.70/5	0.537(7)	0.135(8)	-0.069(5)	0.39(7)
	32	10.06/4	0.527(7)	0.123(7)	-0.068(4)	0.5(1)
P ₃	16	1.69/6	0.516(1)	0.1007(6)	-0.147(8)	1.08(4)
	24	1.64/5	0.516(2)	0.1006(9)	-0.15(2)	1.10(8)
	32	0.95/4	0.513(3)	0.099(1)	-0.2(1)	1.3(2)
	48	0.29/3	0.52(1)	0.103(8)	-0.07(8)	0.8(6)
P ₄	64	0.18/2	0.51(1)	0.100(6)	-0.3(15)	1.3(17)
	16	13.29/6	0.514(1)	0.0849(6)	-0.088(5)	0.98(4)
	24	6.88/5	0.511(1)	0.0834(7)	-0.12(2)	1.16(8)
	32	6.59/4	0.512(3)	0.084(2)	-0.10(5)	1.1(2)

Table VII. Fits of ξ_y to Eq. (5) for a y line in the LR ordered phase.

Parameters	L_{\min}	χ^2/DOF	q	a	b	ω	c
P ₁	8	1.97/6	0.533(2)	0.117(1)	0.61(5)	1.86(6)	0.093(5)
	16	1.19/5	0.530(4)	0.119(4)	0.4(2)	1.6(3)	0.08(2)
	24	1.12/4	0.53(1)	0.121(9)	0.3(3)	1.5(8)	0.07(5)
P ₂	8	13.50/6	0.534(2)	0.142(2)	0.51(7)	1.9(1)	0.157(5)
	16	8.42/5	0.52(1)	0.16(1)	0.20(7)	0.9(4)	0.1(1)
P ₃	8	1.52/6	0.522(3)	0.185(3)	1.38(7)	1.73(5)	0.10(1)
	16	1.44/5	0.521(6)	0.187(7)	1.3(4)	1.7(2)	0.09(3)
	24	1.27/4	0.52(1)	0.19(2)	0.9(7)	1.5(6)	0.1(1)
P ₄	8	12.37/6	0.518(2)	0.231(4)	1.26(7)	1.68(5)	0.11(1)
	16	7.47/5	0.505(9)	0.25(2)	0.74(9)	1.2(2)	-0.01(9)
	24	6.89/4	0.51(1)	0.24(2)	1.4(14)	1.6(6)	0.09(8)

Table VIII. Fits of R to Eq. (6) for a y line in the LR ordered phase.

Parameters	L_{\min}	χ^2/DOF	a	b	ω
P ₁	16	57.76/7	0.67596(2)	0.092(1)	0.876(5)
	24	17.26/6	0.67581(3)	0.081(2)	0.830(9)
	32	8.09/5	0.67572(5)	0.075(3)	0.80(1)
	48	2.67/4	0.67556(9)	0.062(5)	0.74(3)
	64	1.91/3	0.6755(1)	0.055(9)	0.71(5)
	80	1.12/2	0.6756(2)	0.07(2)	0.78(9)
	96	0.81/1	0.6755(4)	0.05(3)	0.7(2)
P ₂	16	11.10/7	0.72684(3)	0.0996(5)	0.656(2)
	24	10.57/6	0.72681(4)	0.0991(8)	0.654(3)
	32	7.72/5	0.72676(5)	0.098(1)	0.648(5)
	48	7.00/4	0.72670(9)	0.095(3)	0.64(1)
	64	0.96/3	0.7264(1)	0.086(4)	0.60(2)
	80	0.92/2	0.7264(3)	0.084(9)	0.60(3)
	96	0.91/1	0.7264(4)	0.09(2)	0.60(5)
P ₃	16	41.96/7	0.77188(1)	0.222(4)	1.345(7)
	24	16.34/6	0.77182(2)	0.178(8)	1.27(2)
	32	3.65/5	0.77175(3)	0.13(1)	1.18(3)
	48	0.41/4	0.77168(5)	0.09(2)	1.07(7)
	64	0.14/3	0.77165(9)	0.07(3)	1.0(1)
	80	0.10/2	0.7716(1)	0.06(6)	1.0(2)
	96	0.01/1	0.7716(3)	0.04(7)	0.9(4)
P ₄	16	55.36/7	0.80148(1)	0.133(3)	1.247(8)
	24	38.21/6	0.80143(2)	0.111(5)	1.19(2)
	32	13.99/5	0.80135(3)	0.079(6)	1.08(3)
	48	12.32/4	0.80130(5)	0.06(1)	1.00(6)
	64	2.45/3	0.8011(1)	0.022(7)	0.7(1)
	80	0.92/2	0.8008(4)	0.011(6)	0.5(2)
	96	0.49/1	0.8010(3)	0.02(2)	0.7(3)

Table IX. Fits of ξ'_y to Eq. (7) for the V plane in the LR ordered phase.

Parameters	L_{\min}	χ^2/DOF	a	q'	b
P ₁	16	17.09/7	0.595(2)	0.4961(7)	-0.154(5)
	24	15.15/6	0.600(4)	0.495(1)	-0.166(10)
	32	11.97/5	0.590(7)	0.498(2)	-0.14(2)
	48	9.80/4	0.57(1)	0.502(4)	-0.09(4)
	64	3.26/3	0.52(2)	0.516(6)	0.06(7)
	80	0.34/2	0.47(4)	0.53(1)	0.3(1)
	96	0.17/1	0.45(6)	0.54(2)	0.3(2)
P ₂	16	8.82/7	0.751(3)	0.4892(7)	-0.313(6)
	24	8.46/6	0.754(5)	0.489(1)	-0.32(1)
	32	6.85/5	0.745(9)	0.491(2)	-0.30(2)
	48	1.89/4	0.71(2)	0.498(4)	-0.20(5)
	64	1.87/3	0.71(3)	0.497(6)	-0.22(9)
	80	1.85/2	0.71(5)	0.50(1)	-0.2(2)
	96	1.40/1	0.66(8)	0.51(2)	-0.0(3)
P ₃	16	43.58/7	0.520(3)	0.5215(9)	0.237(6)
	24	10.01/6	0.544(5)	0.514(2)	0.18(1)
	32	9.69/5	0.548(9)	0.513(3)	0.17(2)
	48	9.69/4	0.55(2)	0.513(5)	0.17(5)
	64	0.46/3	0.48(3)	0.533(8)	0.40(9)
	80	0.44/2	0.47(5)	0.53(1)	0.4(2)
	96	0.12/1	0.44(7)	0.55(2)	0.6(3)
P ₄	16	29.01/7	0.680(3)	0.5088(9)	0.043(7)
	24	15.01/6	0.699(6)	0.504(2)	-0.00(1)
	32	13.37/5	0.71(1)	0.502(3)	-0.03(3)
	48	12.93/4	0.70(2)	0.504(5)	0.00(6)
	64	12.90/3	0.69(4)	0.505(8)	0.0(1)
	80	12.54/2	0.73(7)	0.50(1)	-0.1(2)
	96	4.04/1	0.50(8)	0.55(2)	0.8(3)

Table X. Fits of ξ_x to Eq. (8) for an x line in the critical phase.

Parameters	L_{\min}	χ^2/DOF	a	b	ω
P ₁	32	12.30/5	0.810(4)	-0.748(10)	0.400(9)
	48	8.33/4	0.800(6)	-0.80(3)	0.44(2)
	64	5.59/3	0.788(8)	-0.91(8)	0.49(4)
	80	0.60/2	0.770(8)	-1.4(3)	0.62(7)
	96	0.19/1	0.76(1)	-1.7(7)	0.7(1)
P ₂	32	17.67/5	0.808(3)	-0.74(1)	0.47(1)
	48	6.87/4	0.796(4)	-0.87(5)	0.54(2)
	64	2.02/3	0.786(5)	-1.1(2)	0.62(5)
	80	1.94/2	0.788(9)	-1.0(3)	0.60(9)
	96	1.06/1	0.78(1)	-1.6(9)	0.7(2)
P ₃	32	45.36/5	1.36(2)	-1.121(4)	0.230(8)
	48	4.78/4	1.24(2)	-1.20(2)	0.32(2)
	64	1.41/3	1.21(2)	-1.31(8)	0.38(3)
	80	0.18/2	1.25(5)	-1.2(1)	0.32(6)
	96	0.17/1	1.24(8)	-1.2(2)	0.3(1)
P ₄	32	30.99/5	1.250(8)	-1.073(8)	0.325(9)
	48	4.09/4	1.19(1)	-1.25(5)	0.41(2)
	64	4.09/3	1.19(2)	-1.24(10)	0.41(4)
	80	3.19/2	1.22(4)	-1.1(1)	0.36(7)
	96	0.02/1	1.16(3)	-1.7(6)	0.5(1)

Table XI. Fits of ξ_x to Eq. (9) for an x line in the critical phase.

Parameters	L_{\min}	χ^2/DOF	a	b	ω
P ₁	32	24.57/5	1.03(2)	-0.908(6)	0.65(4)
	48	12.24/4	0.92(2)	-0.96(3)	0.93(9)
	64	7.02/3	0.86(2)	-1.2(1)	1.3(2)
	80	0.79/2	0.80(2)	-2.3(8)	2.0(3)
	96	0.14/1	0.79(2)	-3.7(27)	2.4(6)
P ₂	32	32.66/5	0.92(1)	-0.82(1)	0.93(5)
	48	10.43/4	0.85(1)	-1.08(9)	1.4(1)
	64	2.30/3	0.82(1)	-1.7(4)	1.9(2)
	80	2.30/2	0.82(2)	-1.7(8)	1.9(4)
	96	1.19/1	0.80(2)	-3.7(35)	2.6(8)
P ₃	48	6.88/4	1.9(2)	-1.8(1)	0.43(7)
	64	0.91/3	1.5(1)	-1.68(4)	0.7(2)
	80	0.17/2	1.7(4)	-1.7(2)	0.5(3)
P ₄	96	0.14/1	1.6(5)	-1.66(5)	0.6(5)
	32	46.61/5	2.1(1)	-1.8(1)	0.34(4)
	48	4.48/4	1.43(5)	-1.51(3)	0.84(9)
	64	4.11/3	1.39(7)	-1.6(1)	0.9(2)
	80	3.57/2	1.5(2)	-1.45(8)	0.7(3)
	96	0.04/1	1.24(8)	-2.7(16)	1.6(6)

Table XII. Fits of G_x to Eq. (10) for an x line in the critical phase.

Parameters	L_{\min}	χ^2/DOF	a	l_0	\hat{q}
P ₁	32	30.56/5	0.613(2)	6.8(3)	0.063(2)
	48	3.39/4	0.598(2)	11.5(10)	0.049(2)
	64	2.19/3	0.594(4)	13.8(23)	0.045(4)
	80	0.18/2	0.61(2)	7.6(45)	0.06(1)
	96	0.10/1	0.62(4)	5.7(75)	0.06(3)
P ₂	32	7.49/5	0.651(2)	7.1(4)	0.050(1)
	48	2.10/4	0.643(3)	9.5(11)	0.044(3)
	64	2.00/3	0.645(6)	8.8(24)	0.045(5)
	80	1.45/2	0.638(9)	12.4(56)	0.039(8)
	96	1.08/1	0.65(3)	7.1(92)	0.05(2)
P ₃	32	17.22/5	0.754(1)	7.2(3)	0.0437(9)
	48	8.31/4	0.748(2)	9.5(8)	0.039(2)
	64	5.76/3	0.742(3)	12.1(19)	0.035(3)
	80	0.27/2	0.732(4)	20.9(42)	0.026(3)
	96	0.14/1	0.730(6)	23.6(84)	0.025(5)
P ₄	32	17.33/5	0.774(1)	7.3(3)	0.0361(8)
	48	10.95/4	0.769(2)	9.4(9)	0.032(2)
	64	3.77/3	0.761(3)	14.3(21)	0.026(2)
	80	1.01/2	0.755(3)	21.3(46)	0.021(3)
	96	0.04/1	0.76(1)	13.2(92)	0.027(8)

Table XIII. Fits of G_x to Eq. (11) for an x line in the critical phase.

Parameters	L_{\min}	χ^2/DOF	a	\tilde{q}
P ₁	8	89646.95/9	0.69645(6)	0.04380(3)
	16	22113.65/8	0.68110(8)	0.03750(4)
	24	6205.57/7	0.6704(1)	0.03334(5)
	32	2340.91/6	0.6635(2)	0.03079(6)
	48	566.30/5	0.6500(4)	0.0261(1)
	64	162.15/4	0.6422(5)	0.0234(2)
	80	22.54/3	0.6343(8)	0.0208(3)
	96	6.28/2	0.631(1)	0.0199(4)
	128	0.93/1	0.627(2)	0.0187(6)
P ₂	8	56517.93/9	0.72069(6)	0.03477(3)
	16	14980.50/8	0.70846(8)	0.02993(3)
	24	4356.30/7	0.6999(1)	0.02673(5)
	32	1790.05/6	0.6945(2)	0.02483(6)
	48	351.83/5	0.6824(4)	0.0208(1)
	64	87.37/4	0.6763(5)	0.0188(2)
	80	27.51/3	0.6715(8)	0.0174(3)
	96	6.30/2	0.668(1)	0.0164(3)
	128	0.13/1	0.664(2)	0.0152(6)
P ₃	8	208791.30/9	0.83314(4)	0.03306(2)
	16	44483.15/8	0.81733(6)	0.02761(2)
	24	11613.20/7	0.80762(8)	0.02440(3)
	32	3702.87/6	0.8008(1)	0.02228(4)
	48	695.83/5	0.7883(2)	0.01865(8)
	64	211.78/4	0.7822(4)	0.0169(1)
	80	80.33/3	0.7765(6)	0.0154(2)
	96	26.34/2	0.7721(9)	0.0142(2)
	128	2.28/1	0.766(2)	0.0126(4)
P ₄	8	152356.56/9	0.84009(4)	0.02711(1)
	16	33838.30/8	0.82727(5)	0.02274(2)
	24	8348.08/7	0.81861(8)	0.01994(3)
	32	2908.44/6	0.8133(1)	0.01833(3)
	48	560.63/5	0.8029(2)	0.01537(7)
	64	201.09/4	0.7978(4)	0.0140(1)
	80	66.35/3	0.7925(6)	0.0126(2)
	96	12.06/2	0.7886(8)	0.0115(2)
	128	0.42/1	0.785(1)	0.0105(4)